

# Earth and Space Science



## RESEARCH ARTICLE

10.1029/2021EA001762

### Key Points:

- Seasonal variations of NO<sub>x</sub> and O<sub>3</sub> at ZOTTO in Siberia show a signature of weakly polluted air due to the regional pollution
- Origins of clean and polluted air for the site are identified; seasonal cycle of the baseline ozone for central North Eurasia is estimated
- In spring-summer, anthropogenic and fire emissions in Siberia provide a net source for tropospheric ozone in the NH midlatitudes

### Correspondence to:

K. B. Moiseenko,  
konst.dvina@gmail.com

### Citation:

Moiseenko, K. B., Vasileva, A. V., Skorokhod, A. I., Belikov, I. B., Repin, A. Yu., & Shtabkin, Yu. A. (2021). Regional impact of ozone precursor emissions on NO<sub>x</sub> and O<sub>3</sub> levels at ZOTTO Tall Tower in central Siberia. *Earth and Space Science*, 8, e2021EA001762. <https://doi.org/10.1029/2021EA001762>

Received 22 MAR 2021

Accepted 11 JUN 2021




### Author Contributions:

**Conceptualization:** K. B. Moiseenko  
**Data curation:** I. B. Belikov  
**Formal analysis:** K. B. Moiseenko, A. V. Vasileva  
**Funding acquisition:** A. I. Skorokhod, A. Yu. Repin  
**Investigation:** K. B. Moiseenko, A. V. Vasileva, Yu. A. Shtabkin  
**Methodology:** K. B. Moiseenko  
**Project Administration:** K. B. Moiseenko, A. I. Skorokhod, A. Yu. Repin

© 2021. The Authors. Earth and Space Science published by Wiley Periodicals LLC on behalf of American Geophysical Union.

This is an open access article under the terms of the [Creative Commons Attribution-NonCommercial-NoDerivs License](#), which permits use and distribution in any medium, provided the original work is properly cited, the use is non-commercial and no modifications or adaptations are made.

## Regional Impact of Ozone Precursor Emissions on NO<sub>x</sub> and O<sub>3</sub> Levels at ZOTTO Tall Tower in Central Siberia

K. B. Moiseenko<sup>1</sup> , A. V. Vasileva<sup>1</sup> , A. I. Skorokhod<sup>1</sup>, I. B. Belikov<sup>1</sup>, A. Yu. Repin<sup>2</sup>, and Yu. A. Shtabkin<sup>1</sup> 

<sup>1</sup>A. M. Obukhov Institute of Atmospheric Physics, Russian Academy of Sciences, Moscow, Russia, <sup>2</sup>E. K. Fedorov Institute of Applied Geophysics, Moscow, Russia

**Abstract** Seasonal variations of the near-surface NO<sub>x</sub> (= NO + NO<sub>2</sub>) and ozone (O<sub>3</sub>) mixing ratios at Zotino Tall Tower (ZOTTO), a remote site in central Siberia, are described for years 2007–2014. Conditional probability function analysis and back trajectories are used to determine the origins of clean (continental baseline, CB) and regional emissions-influenced air. High NO<sub>x</sub> levels at the site are observed for air from industrial regions of western Siberia and Ural Mountains, whereas CB air originates from remote areas of North Eurasia within 55°–70°N. The estimated annual means of daytime O<sub>3</sub> and NO<sub>x</sub> mixing ratios for CB air are 27.0 and 0.44 ppbv, correspondingly, versus the similar quantities of 27.9 and 0.79 ppbv for all data. Monthly ozone for CB air shows a distinct maximum in April, as is the case for Northern Hemisphere midlatitude baseline (NHMLB) air at the European inflow boundary according to the surface ozone data for Mace Head and Norwegian monitoring sites, and a minimum in late summer–early autumn reflecting a weak continental-scale ozone production from biogenic sources of ozone precursors and wildfire emissions throughout the warm season. During spring and early summer under hot weather conditions, regional anthropogenic and wildfire emissions are an important source for ozone in the continental boundary layer over southern and central Siberia, resulting in surface ozone levels compared to or larger than those observed in NHMLB air. Throughout the remaining part of year, the central North Eurasia represents a sink for tropospheric ozone on a hemispheric scale.

## 1. Introduction

Measurements of ozone (O<sub>3</sub>) and its precursors, including NO<sub>x</sub> species (NO<sub>x</sub> = NO + NO<sub>2</sub>), allow assessment of the current state of the tropospheric photochemical system (TPS), as well as long-term trends in chemical air composition associated with the changing climate and strength of air pollution sources. Ozone is a key compound of the TPS, whose photolysis initiates most of the chemical reactions through generating an excited atomic oxygen O(<sup>1</sup>D). A subsequent reaction of O(<sup>1</sup>D) with a molecule of water (H<sub>2</sub>O) is the principal source for the tropospheric hydroxyl radical OH which drives oxidation of relatively stable ozone precursor species [e.g., carbon monoxide (CO), methane (CH<sub>4</sub>), and higher molecular mass hydrocarbons (NMHC)] emitted from various natural and anthropogenic sources. Also, O<sub>3</sub> is an important secondary pollutant whose mixing ratios above 40–60 ppbv are harmful to human health (Atkinson et al., 2016; Kotelnikov et al., 2017; Turner et al., 2016), crops (Fuhrer, 2009; Hollaway et al., 2012; Mills et al., 2007), and natural vegetation (Arnold et al., 2018; Cailleret et al., 2018; Mills et al., 2011 and references therein). Finally, ozone, being the third most important man-made greenhouse gas after carbon dioxide and CH<sub>4</sub>, affects carbon sequestration (Felzer et al., 2005; Wang et al., 2016) and atmospheric radiation properties (Myhre et al., 2013). Oxidation of CO, CH<sub>4</sub>, and NMHC in the atmosphere occurs via chemical chain reactions with NO<sub>x</sub>, which is the rate-limiting precursor in relatively unpolluted air (Kleinman et al., 1997; Lin et al., 1988), whereas chemical sink of NO<sub>x</sub> into more stable reactive nitrogen species [e.g., nitric acid (HNO<sub>3</sub>), alkyl, multifunctional organic nitrates, etc.] and their subsequent removal from the atmosphere through deposition and hydrolysis limit the lifetime of NO<sub>x</sub> in the lower troposphere by a few hours or days (Browne & Cohen, 2012; Kenagy et al., 2018; F. Liu et al., 2016), thus limiting total ozone production on a regional scale. Hence, observations of O<sub>3</sub> and NO<sub>x</sub> levels in baseline air far from local pollution sources allow for some conclusions on the overall abundance of secondary pollutants in the air and the net ozone production potential of the regional pollutant emissions. From this point of view, simultaneous measurements of the above species at remote continental and marine sites are

**Resources:** A. I. Skorokhod, I. B. Belikov, A. Yu. Repin  
**Software:** A. V. Vasileva, I. B. Belikov, Yu. A. Shtabkin  
**Supervision:** A. I. Skorokhod, A. Yu. Repin  
**Validation:** A. V. Vasileva, I. B. Belikov, Yu. A. Shtabkin  
**Visualization:** A. V. Vasileva  
**Writing – original draft:** K. B. Moiseenko  
**Writing – review & editing:** A. V. Vasileva

of special interest, being representative for large geographical areas and characterizing some features of the reference state TPS (Derwent et al., 1998; Oltmans, 1981; Parrish et al., 2013; Singh et al., 1978).

In the present study, we describe the seasonal cycles of  $O_3$  and  $NO_x$  at Zotino Tall Tower Observatory (ZOTTO; Heimann et al., 2014; Kozlova & Manning, 2009), a remote station in central Siberia that has been put into operation in October 2006, as a joint project between the Max Planck Institute of Biogeochemistry, Jena (Germany), and the I. V. Sukachev Institute of Forest, Siberian Branch of the Russian Academy of Sciences, Krasnoyarsk (Russia). The site is perfectly placed to study ozone photochemistry in the continental boundary layer (CBL) under baseline and polluted conditions. Spatial localization of major source regions for odd nitrogen and ozone is performed through the Conditional Probability Function analysis (Ashbaugh et al., 1985; Vasconcelos et al., 1996) coupled with 3-days Lagrangian (kinematic) back trajectories to determine the origins of clean and polluted air for ZOTTO. Ozone levels for the continental baseline (CB) and regional emissions-influenced (REI) air masses are then analyzed to quantify the impact of regional pollution sources on the abundance of ozone in the lower troposphere over remote North Eurasia and assess the importance of Siberia as a net sink or source for tropospheric ozone on continental and hemispheric scales.

## 2. Data Sets and Analysis

### 2.1. The ZOTTO Site

The research site (<http://www.zottoproject.org>) (60° 48'N, 89° 21'E, 114masl) is located in central Siberia on the eastern edge of the West Siberian Lowland, ~20 km west of the Zotino settlement on the Yenisey River (star symbol in Figure 1). The surrounding vegetation is a mixture of bogland and boreal coniferous forest. The local climate is strongly continental with a large annual temperature cycle. The diurnal temperatures range from 30°C in summer to –40°C in winter. The climatological wind rose at the nearby weather station shows an appreciable change in direction of the prevailing winds from S and SW in winter to the NW quadrant in summer, reflecting seasonal variations in circulation patterns over Siberia (Eneroth et al., 2003; Heimann et al., 2014). Consequently, the most significant sources of atmospheric contamination affecting the site are large towns and industry in West Siberia (~500–1,000km SSE to NW from the site), as well as steppe and forest fires in northern Kazakhstan and southern Siberia (Chi et al., 2013; Mikhailov et al., 2017; Thorp et al., 2020). On a yearly basis, clean air is measured at the site for approximately half of the time, with the longest periods of near-pristine conditions observed in summer months due to the seasonal shift in the prevailing air transport pathways to the northern latitudes and the shorter atmospheric residence times of pollutant species in CBL in this period of the year (Mikhailov et al., 2017).

### 2.2. $NO_x$ and $O_3$ Data

Ozone was measured with Dasibi 1008-AH or 1008-RS UV photometric gas analyzers having a measurement range of 1–1,000 ppbv and an estimated precision of the original 1min data of ~1ppbv at ozone levels well above the detection limit. Nitrogen oxides were measured with Thermo Fisher Scientific TE42C-TL instrument. The method is based on the luminescence radiation from the chemical reaction between NO and  $O_3$ . To measure  $NO_2$ , a catalytic converter reducing  $NO_2$  to NO was used. The instrument has a response time of 60s and overall uncertainty of  $\pm 1\%$  for measured NO and  $NO_2$  mixing ratios well above the detection limit of 0.05°ppbv. The 1min  $O_3$ , NO, and  $NO_2$  data were filtered for spurious impact of local pollution sources seen as strong short-period fluctuations in the measured species mixing ratios (93% of data capture). The filtered data have been aggregated to 1°h averages centered at 00:00, 01:00, ..., 23:00 UTC provided both  $O_3$  and  $NO_x$  data cover at least half of the respective hour. The afternoon means (12:00–18:00 local time) of hourly  $NO_x$  and  $O_3$  mixing ratios for the whole observation period from March 2007 to December 2014, which are further referred to as *daily data*, are used to study the  $O_3$ – $NO_x$  correlations and source–receptor relationships for the site. The daily mixing ratios seem to be most appropriate for characterizing the combined effect of vertical mixing in the boundary layer and photochemistry during sunlight hours, the processes which are not separated straightforwardly based on the present observations.

Air inlets, which were plastic funnels directed downwards, were located on the ZOTTO tower at a height of 6.7 m above ground level. Air from inlets was supplied to the analyzers via Teflon pipelines with 1/8" internal

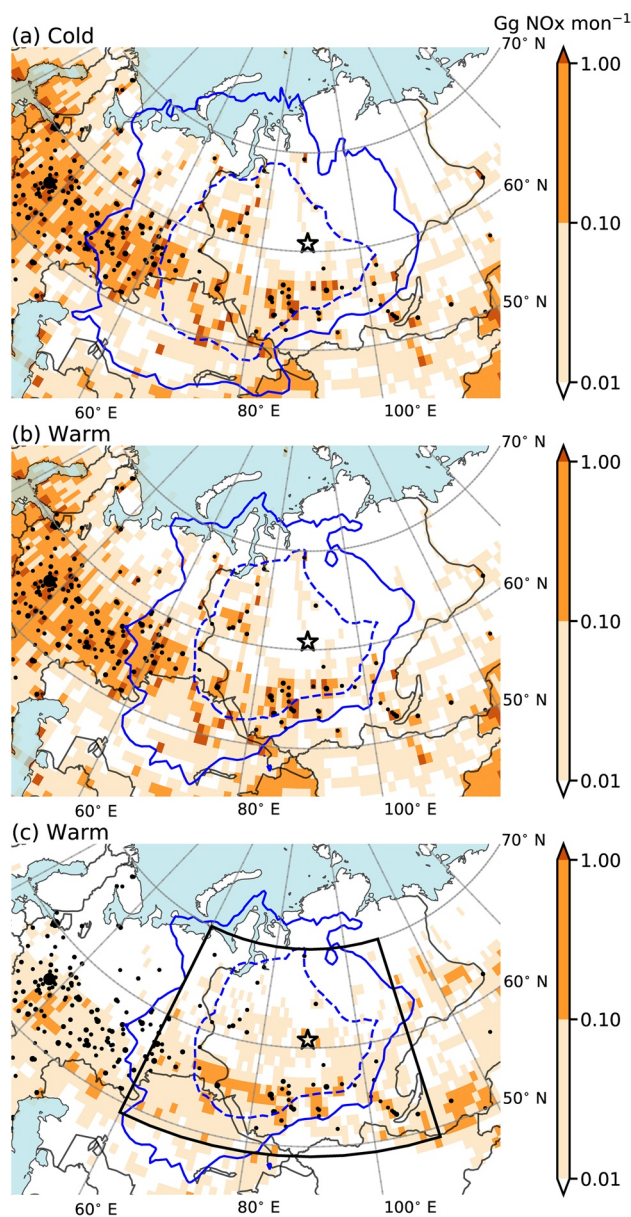


**Figure 1.** Contour map of SCF values (0.1: solid blue line, 2.0: dashed blue line, see Section 2.4) outlining the areas of 3-days-long air transport to ZOTTO, against the monthly average (a and b) anthropogenic and (c) wildfire  $\text{NO}_x$  emissions (color bar,  $10^9 \text{ g NO}_x$ ) on a  $1^\circ \times 1^\circ$  grid in (a) cold (October–March) and (b and c) warm (April–September) seasons of 2007–2014. Black dots are the cities with population  $>50,000$  according to [naturalearthdata.com](http://naturalearthdata.com); star symbol is the ZOTTO site; black rectangle in (c) is the region for which total  $\text{NO}_x$  emissions are provided in Figure 5.

diameter and 10 m long. For each instrument ( $\text{O}_3$  and  $\text{NO}$ ,  $\text{NO}_2$  measurements), a separate pipeline was used. The airflow of the instruments was  $2.0 \text{ l min}^{-1}$  for  $\text{O}_3$  measurements and  $1.3 \text{ l min}^{-1}$  for  $\text{NO}$ ,  $\text{NO}_2$ . Air sampling was carried out with the original instrument pumps, with no additional pumps used. With the specified parameters, the Reynolds number is about 1,000, and the Poiseuille formula is valid for the laminar flow, so the maximum pressure drop across the pipeline is not more than 30 mbar, which does not go beyond the acceptable limits for the instruments used.

The  $\text{O}_3$  instrument was calibrated annually against a secondary standard, which was the O341 M instrument calibrated annually according to the SPR #38 standard owned by the Mendelev Research Metrology Institute (Russia). The  $\text{NO}$ ,  $\text{NO}_2$  instrument was calibrated annually with the gas standards provided by the Mendelev Research Metrology Institute. In addition, during the measurements, weekly checks of the  $\text{NO}$ ,  $\text{NO}_2$  instrument zero level were carried out using a high purity compressed nitrogen cylinder. Regular checks of the  $\text{NO}$ ,  $\text{NO}_2$  instrument zero level for  $\text{NO}$  were also carried out when processing observational data, taking into account the fact that nighttime  $\text{NO}$  concentrations were usually below the detection limit of the instrument.

### 2.3. Trajectory Model

Ensembles of three-dimensional 5-day backward Lagrangian air parcel trajectories were generated with the earlier developed computational code (Vasileva et al., 2011), which utilizes the ERA-Interim  $0.75^\circ \times 0.75^\circ$  6 h meteorological data. For each day, the calculations were conducted every hour from 00:00 to 23:00 starting from pressure levels of 950, 925, 900, and 875 hPa (400–1,000 m agl at ZOTTO) by varying additionally the ground location (the ZOTTO coordinates  $\pm 0.25^\circ$  latitude or longitude), with the trajectory segment endpoints saved at the  $\Delta t = 30 \text{ min}$  time increment. The above range of starting (in backward direction) altitudes is chosen to constrain the regional pattern of low-level air mass transport, to which the results of the present source–receptor analysis are found to be most sensitive. Varying trajectory duration time,  $\tau_t$ , from 2 to 5 days or limiting the range of starting heights to 950–900 hPa does not lead to any appreciable change in our final estimates, so below we discuss the results of simulations for the optimal value of  $\tau_t = 3$  days, as it provides the best agreement between the model-predicted source area for the site and the regional pattern of anthropogenic and wildfire  $\text{NO}_x$  emissions.

### 2.4. Source–Receptor Relationship

Air masses arriving at ZOTTO have been sorted into *clean* and *polluted* categories according to the measured  $\text{NO}_x$  levels. Subtracting the median of daily  $[\text{NO}_x]$  values (here and after,  $[\cdot]$  is a species mixing ratio in ppbv) in the  $\pm 8$  days running window from the original data, we obtain a *synoptic* part of the  $\text{NO}_x$  time series ( $\text{NO}_x'$ ), containing short-term variations with the periods of 2–16 days. The corresponding special-case subsets  $\{\text{NO}_x'\}_L$  and  $\{\text{NO}_x'\}_H$  of low and high  $\text{NO}_x'$  values from the whole time series  $\{\text{NO}_x'\}$  of daily fluctuations were then derived based on the predefined threshold values  $[\text{NO}_x']_L$  and  $[\text{NO}_x']_H$  (see details at the end of this section), marking the transition between clean,  $[\text{NO}_x'] \leq [\text{NO}_x']_L$ , and polluted,  $[\text{NO}_x'] \geq [\text{NO}_x']_H$ , air.

Spatial localization of the origins of clean and polluted air at ZOTTO is performed with the residence time analysis according to Ashbaugh et al. (1985) and Vasconcelos et al. (1996). The residence time of air parcels,



traveling to the receptor during the time interval  $\tau_i$  (defined in Section 2.3), is calculated on a regular  $1^\circ \times 1^\circ$  grid as a product of a time interval  $\Delta t$  between two consequent endpoints and a number  $n_{ij}$  of back trajectory segment endpoints that fall into the grid cell  $ij$ . The grid cells with  $n_{ij} > 0$  comprise a *source area* where emission sources may be potentially significant for the ZOTTO site (Figure 1). The ratio of the residence time of a randomly selected air parcel in the grid cell  $ij$  to the total travel time  $\tau_i$  then represents the probability that the previous position of the parcel is estimated to be in the cell  $ij$  at any time up to the maximum travel time  $\tau_i$ . The corresponding residence time probability density function, divided by another probability density function resulting from a hypothetical trajectory distribution with constant wind velocity and radial symmetry centered at the receptor, is employed in our study to construct the discrete *Source Contribution Function* (SCF) shown in Figure 1, following the methods of Ashbaugh et al. (1985).

We also calculate special case residence times using a number  $n_{ij}^*$  of endpoints that fall into the grid cell  $ij$  and belong to a trajectory with arrival time corresponding to the  $\{\text{NO}_x'\}_L$  or  $\{\text{NO}_x'\}_H$  subsets of  $\text{NO}_x$  mixing ratios observed at the receptor. The ratio of the residence time and the special case residence time for each grid cell  $ij$  estimates the *Conditional Probability* (CP) that a randomly selected air parcel crossing the grid cell  $ij$  arrives at the receptor with high,  $\{\text{NO}_x'\}_H$ , or low,  $\{\text{NO}_x'\}_L$ , synoptic-scale fluctuation at the  $\text{NO}_x$  mixing ratio. Thus,  $CP_{ij} = n_{ij}^*/n_{ij}$ , where “\*” is either “L” or “H”. Thus, cells with high and statistically significant CP values are indicative of areas of low (for  $\{\text{NO}_x'\}_L$  subset) and high (for  $\{\text{NO}_x'\}_H$ ) potential regional contributions to  $\text{NO}_x$  mixing ratios at ZOTTO.

Seasonal partitioning of the ZOTTO data has been performed according to the spatial patterns of wildfire activity in Siberia and the observed different relationships between  $\text{O}_3$  and  $\text{NO}_x$  levels in cold and warm seasons (see Section 3.2). Previous studies show that the seasonal cycles of frequency and extent of wildfires in southern Siberia ( $45^\circ$ – $55^\circ\text{N}$ ) have two maxima, in late spring and early autumn, and become unimodal at higher latitudes where they reach maxima in July to August, following the annual cycles of solar radiation, precipitation, and soil thawing (Ponomarev et al., 2016; Vasileva et al., 2010). We then calculate CP fields for each season to better account for spatially varying patterns of wildfire activity in the region and different responses in the regional ozone levels to the  $\text{NO}_x$  emissions attributed to both wildfire and anthropogenic activity. We have validated the source areas of polluted and clean air at ZOTTO, predicted with the CP-based model for different  $[\text{NO}_x']_L$  and  $[\text{NO}_x']_H$  thresholds, with the public databases on EDGARv4.3.2 (Janssens-Maenhout et al., 2019) anthropogenic (Figures 1a and 1b) and GFEDv4.1s (Mu et al., 2011; van der Werf et al., 2017) wildfire (Figure 1c)  $\text{NO}_x$  emissions. We have found the  $\text{NO}_x'$  values in the bottom and top quartiles of  $\{\text{NO}_x'\}$  to be nearly optimal for discriminating clean and polluted conditions, correspondingly, with the remaining half of the observations left unclassified. In either case, the origin of the air masses arriving at ZOTTO is identified as an area covered by a subset of grid cells with  $CP > 0.25$ , the expected conditional frequency in the absence of any association between an air parcel trajectory path and the corresponding measured  $\text{NO}_x$  value from the prescribed quartile of the data (Vasconcelos et al., 1996).

### 3. Results and Discussion

#### 3.1. $\text{O}_3$ and $\text{NO}_x$ Seasonal Cycles

Average seasonal cycles of daily  $\text{O}_3$  and  $\text{NO}_x$  levels at ZOTTO over the 2007–2014 observation period are shown in Figure 2, with the corresponding monthly statistics provided in Table 1. The estimated annual means of daily mixing ratios are 27.9 ppbv for  $\text{O}_3$  and 0.79 ppbv for  $\text{NO}_x$ . The wide range of atmospheric transport pathways to the site (see Figure 1) and weather conditions, as well as different rates of photochemical processing of the polluted air, result in the high observed strong short-term (synoptic) variability of daily  $\text{O}_3$  and  $\text{NO}_x$  levels as suggested by the wide monthly  $P_{05}$ – $P_{95}$  percentile ranges of daily mixing ratios. When averaged over all months of observations, the amplitude of synoptic fluctuations for ozone, calculated as the difference between  $P_{95}$  and  $P_{05}$  percentiles, is 19.2 ppbv, which is comparable to the amplitude of the ozone seasonal cycle (22.6 ppbv) based on the difference between  $\text{O}_3$  median values of 42.3 ppbv in April and 19.7 ppbv in September. The total variation in daily ozone levels is highest from April to July (24.7 ppbv on average), which is also the period of most intense photochemical ozone production from the regional pollutant emissions (see more discussion in Section 3.5). Hence, weather-induced perturbations in

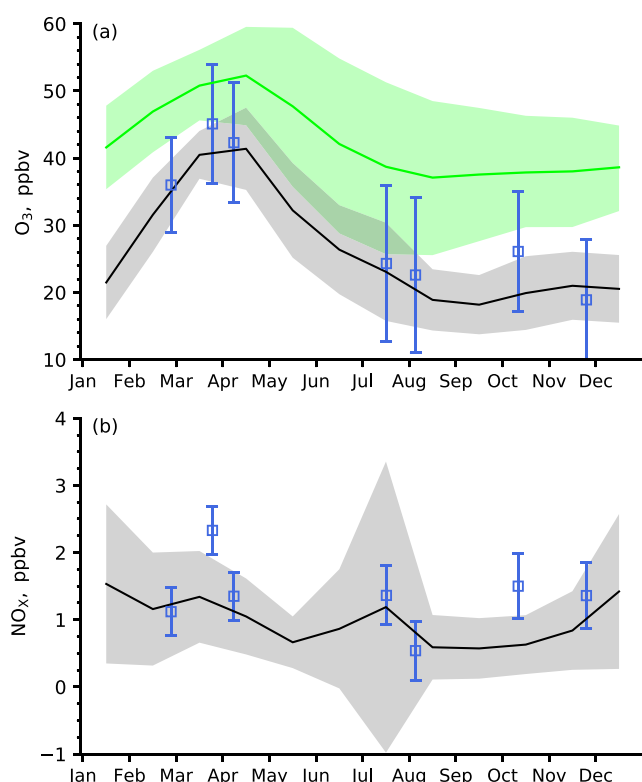


**Figure 2.** Monthly statistics of mean daily (00:00–23:00 LT) (a)  $O_3$  and (b)  $NO_x$  mixing ratios: lines or squares—mean values, filled areas or bars—standard deviations; black is for ZOTTO data for years 2007–2014, green is for Mondy ( $51^{\circ}39'N$ ,  $100^{\circ}55'E$ , 2010 m asl) data for years 1998–2016 according to Potemkin et al. (2019); blue is for data from TROICA campaigns for years 1995–2008 (Elansky, 2009) placed along the X axis according to the representative day of year of the measurements.

**Table 1**

Monthly Statistics of Average Afternoon (12:00–18:00 Local Time)  $O_3$  and  $NO_x$  Mixing Ratios at ZOTTO in Years 2007–2014 as Shown in Figure 2

Months	$O_3$ (ppb)				$NO_x$ (ppb)			
	Mean	Median	$P_{05}$	$P_{95}$	Mean	Median	$P_{05}$	$P_{95}$
1	22.9	23.4	14.0	31.9	1.2	1.0	0.3	2.4
2	33.2	32.9	25.1	41.3	1.0	0.8	0.4	1.9
3	41.3	40.9	35.8	47.7	1.2	1.1	0.6	2.0
4	42.5	42.3	31.5	54.1	1.0	0.8	0.4	1.8
5	33.7	33.7	20.5	44.6	0.6	0.5	0.3	1.2
6	29.5	29.6	17.9	40.5	0.7	0.5	0.2	1.5
7	26.3	25.1	12.3	41.6	0.7	0.4	0.2	1.4
8	21.6	21.8	12.8	30.6	0.4	0.3	0.2	0.9
9	20.1	19.7	12.5	29.0	0.4	0.3	0.1	0.9
10	20.8	20.6	11.9	29.9	0.5	0.4	0.1	1.2
11	21.5	21.8	13.5	29.8	0.7	0.5	0.2	1.6
12	21.0	20.4	13.2	29.9	1.1	0.9	0.4	2.7

local ozone photochemistry are expected to be most important in April to July, resulting in the observed seasonal increase in the ozone variability at the site.

The measured ozone levels at ZOTTO reveal a unimodal seasonal cycle, which has a distinct maximum in April and a flat minimum in August to September. A similar ozone cycle is typical for other baseline midlatitude surface monitoring sites in northwest Europe and North America subjected to minor anthropogenic loading (Chan & Vet, 2010; Derwent et al., 2013; Katragkou et al., 2015; Logan, 1985, 1989; Monks, 2000; Solberg et al., 1997; Vingarzan, 2004). Particularly, the maximum value of 42.5 ppbv in April (Table 1) is very close to the annual maximum of baseline ozone at Mace Head (44 ppbv, see Derwent et al., 2013) and rural Norwegian ozone monitoring sites at similar latitudes ( $41^{\circ}$ – $43^{\circ}$  ppbv,  $60^{\circ}$ – $65^{\circ}$ N, see Solberg et al., 1997), as well as at Zeppelin (42 ppbv), the remote Arctic station at Spitsbergen, Norway (Hirdman et al., 2010).

Compared to the ozone data, a much higher degree of irregularity is observed for a seasonal cycle of  $NO_x$  at the site, with the synoptic fluctuations clearly dominating the total variability of daily  $NO_x$  levels (Figure 2b). Yet, the seasonal cycle of  $NO_x$  at the site is clearly discernible, with monthly medians of  $NO_x$  peaking in the cold season from December to March (0.95 ppbv on average) and reaching a minimum in late summer and early autumn (0.30 ppbv on average for August to September). The observed accumulation of  $NO_x$  in the cold season replicates the seasonal trends of other ozone precursor species ( $CO$ ,  $CO_2$ , and  $CH_4$ ) at ZOTTO (Chi et al., 2013; Lloyd et al., 2002; Timokhina et al., 2018) having large continental sources, whose lower-tropospheric abundance is controlled to large extent by the seasonally varying vertical mixing conditions and rates of photochemical destruction (in the case of  $CO$  and  $CH_4$ ) in CBL and the free troposphere aloft.

In Figure 2, we compare the ZOTTO  $O_3$  and  $NO_x$  data against the corresponding average values for rural and remote air measured in the TROICA expeditions in 1995–2008 along the Trans-Siberian Railroad from Moscow to Vladivostok (see Crutzen et al., 1998; Elansky, 2009 and references therein). Since the measurements were conducted from the moving train, each data point for a particular TROICA campaign shown in Figure 2 represents a combined spatial and temporal average of the in situ mixing ratios for the segments of the TROICA route associated with the areas of weak and moderate anthropogenic loading. Hence, the derived  $O_3$  and  $NO_x$  mixing ratios can be considered to be representative, on a monthly basis, for the vast areas of the continent in the  $48^{\circ}$ – $58^{\circ}$ N latitude belt encompassed by the TROICA measurements. Figure 2 shows essentially the similar seasonal cycles of ozone for ZOTTO and TROICA, with a higher dispersion of the TROICA data attributed most probably to a wide range of local meteorological conditions, precursor emissions, and ozone deposition rates encountered along each measurements route. Somewhat different in Figure 2 are March and October when the average mixing ratios in TROICA exceed those at ZOTTO by 4–6 ppbv for  $O_3$  and by 0.8–1.1 ppbv for  $NO_x$ , which is most likely attributed to the enhanced wildfire activity along a substantial part of the railroad (Vasileva et al., 2017). Yet, the agreement between the monthly ozone levels derived from the intrinsically different

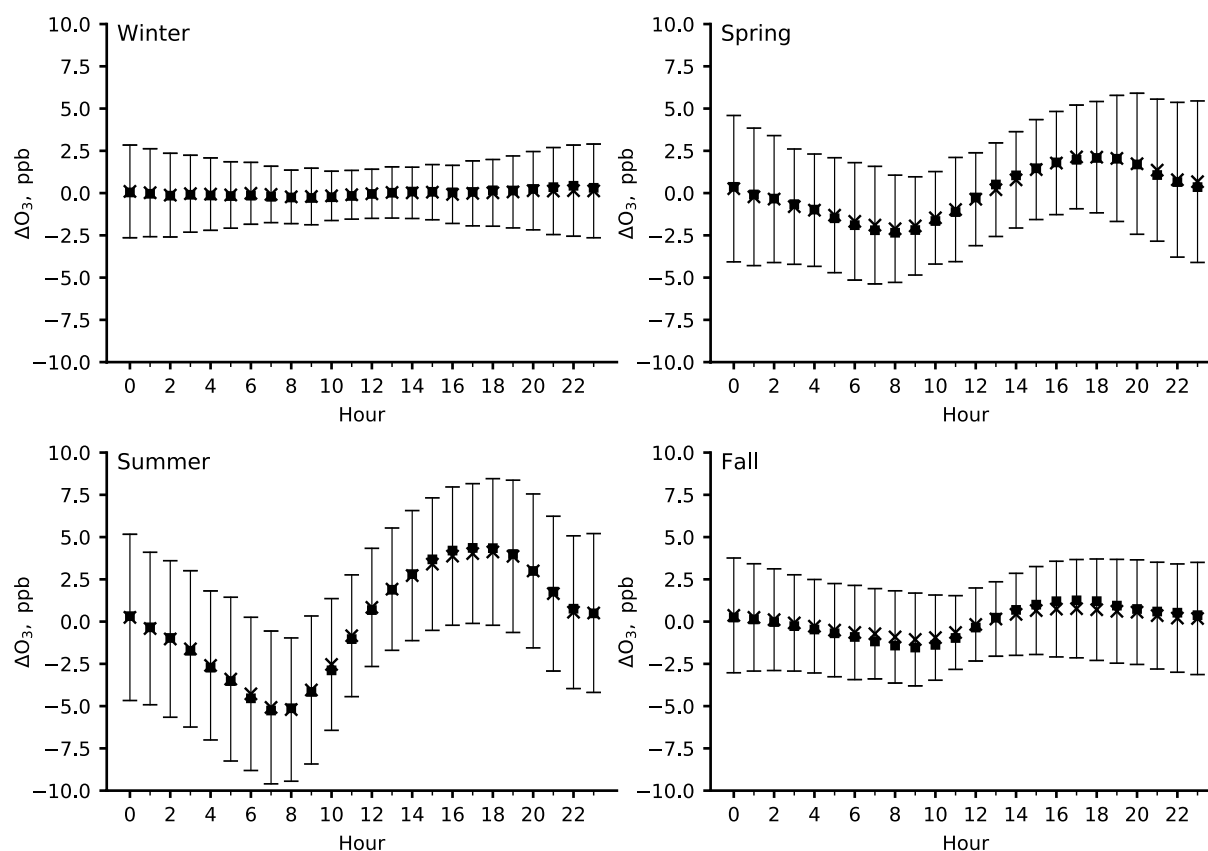


**Figure 3.** Seasonal variability of the ozone diurnal cycle at ZOTTO in 2007–2014: mean (squares), median (crosses), and 1 standard deviation (error bars) of the difference between the 1 h average  $O_3$  mixing ratio and its mean value for the current day of observation.

datasets indicates that the  $O_3$  seasonal cycle observed at ZOTTO is governed by the continental-scale effects of transport, surface deposition, and photochemistry (Elansky, 2009).

The comparison with the published  $O_3$  data at Mondy, an alpine site in the southern Siberia ( $52^\circ N$ ,  $101^\circ E$ , 2006 m asl, see Potemkin et al., 2019), shows the similar phases of the springtime ozone maximum and a 1 month of delay in the seasonal minimum of ozone at ZOTTO, reflecting a prolonged period of active ozone photochemistry in the CBL over Siberia (see below). The most important difference between the two ozone seasonal cycles is systematically higher ozone levels at Mondy, which exceed those at ZOTTO by 10–20 ppbv depending on the season. The equivalent vertical gradient in ozone mixing ratio in the lower 2 km thick atmospheric layer then ranges from  $\sim 5.3$  ppbv  $km^{-1}$  in April to  $\sim 10.6$  ppbv  $km^{-1}$  in early autumn, based on the ground elevations and monthly ozone values at the two sites. The positive vertical gradients of ozone in the lower troposphere over Siberia throughout the photochemically active season from April to September were previously reported by Paris et al. (2008) from the YAK-AEROSIB aircraft campaign in 2006 and by Engvall-Stjernberg et al. (2012) who compared the ZOTTO  $O_3$  data for March 2007 to February 2008, the YAK-AEROSIB airborne measurements in 2006–2008, and the TROICA train-based measurements in 1999–2009.

Also, the amplitude of the ozone seasonal cycle at ZOTTO (21 ppbv) is substantially higher than at Mondy (15 ppbv), based on the April and August monthly averages. Both the higher vertical gradient during the warm season and the larger amplitude of the seasonal cycle of ozone at ZOTTO are explained by the stronger impact of surface deposition at the ZOTTO site, which is located in lowlands, in contrast to the alpine Mondy site. The above conclusion is strongly supported by the significantly higher amplitude of the ozone diurnal cycle observed at ZOTTO (Figure 3), which is approximately two times as much as that for the Mondy site throughout the year (see Potemkin et al., 2019). The other probable reason for the substantially higher ozone levels at Mondy compared to those for ZOTTO during the photochemically active season is a stronger input of distant ozone sources, associated mainly with the industrial regions of Western Europe and the eastern part of Russia (Pochanart et al., 2003). The high location of the Mondy site results both in the

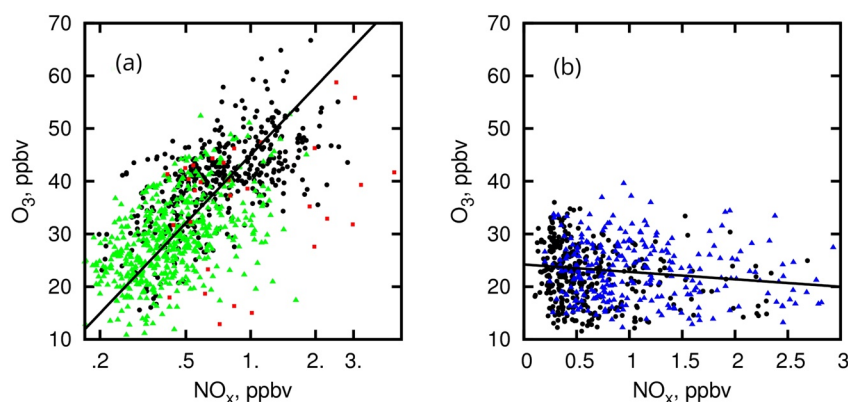


**Figure 4.** The  $O_3$ – $NO_x$  dependence for the central months of each season of the 2007–2014 period: (a) April (black circles) and July (green triangles) data,  $R^2 = 0.55$ ; (b) November (black circles) and January (blue triangles) data,  $R^2 = 0.02$ . The orthogonal least squares fits ( $\pm 2$  standard deviation) are: (a)  $[O_3] = A + B \cdot \log_{10}([NO_x]/1 \text{ ppbv})$ ,  $A = 46.1 (\pm 1.3) \text{ ppbv}$ ,  $B = 37.8 (\pm 3.4) \text{ ppbv}$ ; (b)  $[O_3] = (a) B \cdot [NO_x]$ ,  $A = 24.1 (\pm 1.2) \text{ ppbv}$ ,  $B = 1.4 (\pm 1.10) \text{ ppbv}$ . The data points for June to July 2012, the severe fire season in central Siberia, are shown by red squares and are not used for the fitting.

weaker impact of surface deposition on the lower tropospheric  $O_3$  and  $NO_x$  levels, as well as in shorter travel times of the polluted air from the source regions, with the reported altitudes of transport varying normally within 2–6 km (the median value for the trajectory maximum altitude is 3.2 km). This is contrasted with the results of the present analysis for ZOTTO, showing that only  $\sim 15\%$  of all air masses descend from altitudes above 850 hPa for the 5-day back trajectory duration.

### 3.2. $O_3$ – $NO_x$ Correlations in Warm and Cold Seasons

Figure 4a shows a significant positive correlation ( $R^2 = 0.55$ ) between the logarithm of the daily mixing ratio of  $NO_x$  and the daily  $O_3$  in spring and summer. As far as the measured  $NO_x$  abundance at ZOTTO can be viewed as a proxy for the amount of  $NO_x$  emitted from upwind sources, the observed increase of daytime ozone with the in situ  $[NO_x]$  levels provides observational evidence for photochemical production of ozone within CBL on a regional scale in the warm season. Recent numerical sensitivity experiments conducted with the GEOS-Chem chemical transport model (Moiseenko et al., 2018) for the region of Siberia showed that a 50% reduction in biogenic volatile organic compounds (BVOCs) emissions results in a 1.6 ppbv decrease in the regional ozone levels in summer, whereas a 50% reduction in anthropogenic  $NO_x$  emissions results in a 2.7 ppbv decrease in ozone on average. This evidently suggests a  $NO_x$ -sensitive regime of ozone production on a regional scale in a photochemically active season. Since the  $[O_3]$  is proportional to  $\log[NO_x]$ , the rate of the local increase in  $O_3$  mixing ratio,  $\Delta[O_3]/\Delta[NO_x]$ , is roughly inversely proportional to  $[NO_x]$  value. This can be explained on a qualitative basis by a lower efficiency of local photochemical ozone production from the oxidation of NMHCs per molecule of  $NO_x$  during daylight hours, as well as by incomplete photochemical processing of air at high  $NO_x$  levels, indicative of relatively short transport time to the site. A quadratic dependence of ozone on the logarithm of the trajectory-integrated  $NO_x$  emissions for a broad range of the equivalent  $[NO_x]$  values from  $<0.5$  to  $\sim 10$  ppbv has been proposed earlier by Solberg et al. (1997) to quantify the impact of upwind pollutant sources on ozone levels in the polluted air arriving at Norwegian monitoring sites.

Figure 4a also demonstrates that wildfires immediately around ZOTTO, as is the case for summer 2012, the severe fire season in Siberia, strongly perturb ozone photochemistry resulting in a large scatter of data on the  $NO_x$ – $O_3$  plot. Also, for a fixed  $[NO_x]$  value, daily ozone levels in fire-contaminated air, being well within the noise of the data, are nevertheless lower by about 7 ppbv on average compared to the main body of the data, evidencing for the suppressed ozone production in smoke plumes from nearby fires.

In the cold season from late autumn to early winter, the linear least squares fit of the daily data gives a weak but statistically significant negative slope of  $-1.4 \text{ ppbv } O_3 \text{ ppbv}^{-1} NO_x$ , indicating net photochemical destruc-

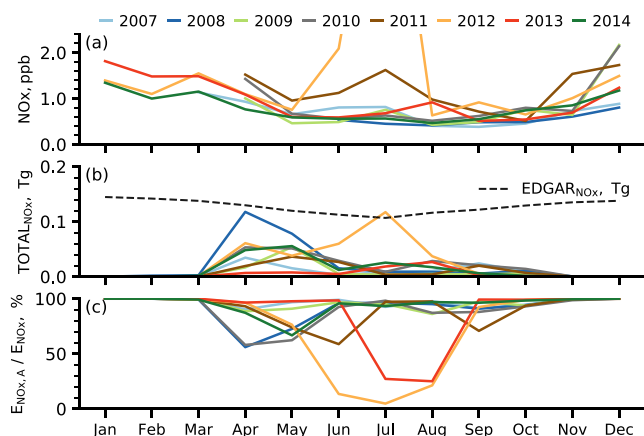


**Figure 5.** Seasonal variations of: (a) monthly mean NO<sub>x</sub> (ppbv) at ZOTTO in 2007–2014 (NO<sub>x</sub> = 7.8 ppbv in July 2012 is beyond the Y axis limit); (b) total monthly biomass burning (GFEDv4.1s, color) and anthropogenic (EDGARv4.3.2, dashed black) NO<sub>x</sub> emissions (Tg) in central North Eurasia (49°–70°N, 60°–110°E, see Figure 1c); (c) fraction of anthropogenic NO<sub>x</sub> input ( $E_{NO_x,A} / (E_{NO_x,A} + E_{NO_x,F})$ ) for the ZOTTO site.

tion of ozone in polluted air via titration by NO<sub>x</sub> and other co-emitted pollutants (Derwent et al., 1998; Parrish et al., 1986; Solberg et al., 1997).

### 3.3. Regional Anthropogenic Versus Fire-Emitted NO<sub>x</sub>

While the instantaneous photochemical ozone production at the measured NO<sub>x</sub> mixing ratios affects significantly the daytime ozone levels at ZOTTO (Moiseenko et al., 2019), the observed correlation between daily afternoon NO<sub>x</sub> and O<sub>3</sub> values reflects, in the most general case, the cumulative effect of ozone chemistry in air mass during its transport from the source area to the site as well. Previous studies (Mikhailov et al., 2017; Vasileva et al., 2011) show that polluted air coming to the ZOTTO site contains commonly a mixture of fire-emitted and anthropogenic pollutants whose individual contributions to the observed O<sub>3</sub> mixing ratios could not be estimated unambiguously for an individual pollution event.

We calculate the total monthly amounts of NO<sub>x</sub> emissions in the source area for ZOTTO (see Section 2.4) by multiplying atmospheric residence time in the cell by monthly NO<sub>x</sub> emission flux (g NO<sub>x</sub> per hour per cell, see color bars in Figure 1) from either anthropogenic sources or wildfires and summing the obtained values over all grid cells. The resulting

monthly inputs from anthropogenic,  $E_{NO_x,A}$ , and wildfire,  $E_{NO_x,F}$ , emissions of NO<sub>x</sub> are shown in Figure 5. One can see that the anthropogenic NO<sub>x</sub> represents the major fraction of the total (defined here as the sum of EDGAR ground-level anthropogenic emissions, without biomass burning, and GFED wildfire emissions) emitted NO<sub>x</sub> in central North Eurasia (50°–70°N, 60°–110°E, see Figures 1c and 5b), as well as within the source area for the site (Figure 5c). The only exception is the summer months of the 2012 and 2013 severe wildfire years in central Siberia, when NO<sub>x</sub> emissions from biomass burning around the ZOTTO site greatly exceeded those from more distant anthropogenic sources. This is contrasted to the regional CO emissions from wildfires which are comparable to, or an order of magnitude higher, than the CO input from anthropogenic sources in years with moderate and severe fire activity in Siberia, correspondingly (Mikhailov et al., 2017; Shtabkin et al., 2016; Vasileva et al., 2011).

A strong prevalence of anthropogenic NO<sub>x</sub> emissions over those from wildfires results in a low NO<sub>x</sub> to CO ratio for a range of biomes typical for Siberia. Also, the predominant pathways of atmospheric transport to the site are from the areas S and SW to the site characterized by the appreciable anthropogenic load and high NO<sub>x</sub> emissions. In the measured NO<sub>x</sub> and O<sub>3</sub> levels at ZOTTO, we then try to separate the effects of total regional anthropogenic and wildfire NO<sub>x</sub> emissions from the effects of continental and hemispheric-scale transport and chemistry which govern the seasonal cycles, through establishing the source–receptor relationship for the site and estimating the ozone seasonal cycles in clean and polluted conditions.

### 3.4. Origins of Clean and Polluted Air for the Site

The gridded CP fields calculated on a seasonal basis for the entire measurement period are shown in Figures 6 and 7 for polluted and clean conditions (as defined in Section 2.4) at ZOTTO. In their study of the atmospheric NO<sub>x</sub> budget in remote CBL including boreal forests, Browne & Cohen (2012) report the *e*-folding time for NO<sub>x</sub> species of 5–12 h in summer. The range of 12–58 h was obtained by Kenagy et al. (2018) for wintertime weakly polluted conditions. Hence, the trajectory length of 3 days used in the present simulations admits a nearly complete photochemical processing of air transported from major regional sources of anthropogenic pollution to the measurements site. According to Figure 6, the polluted air originates mostly from the areas of large anthropogenic NO<sub>x</sub> emissions in southern Siberia, SE to W from the site, throughout the most time of year. Additionally, a contribution of more distant sources from the southern Ural Mountains and European Russia (i.e., the areas west of 60° longitude) is seen distinctly in spring and fall due to more frequent zonal transport in these seasons. In summer, the statistically significant contribution of NO<sub>x</sub> from wildfires in eastern Siberia E and NE to ZOTTO (Figure 1c) is well seen as the enclosed areas in Fig-



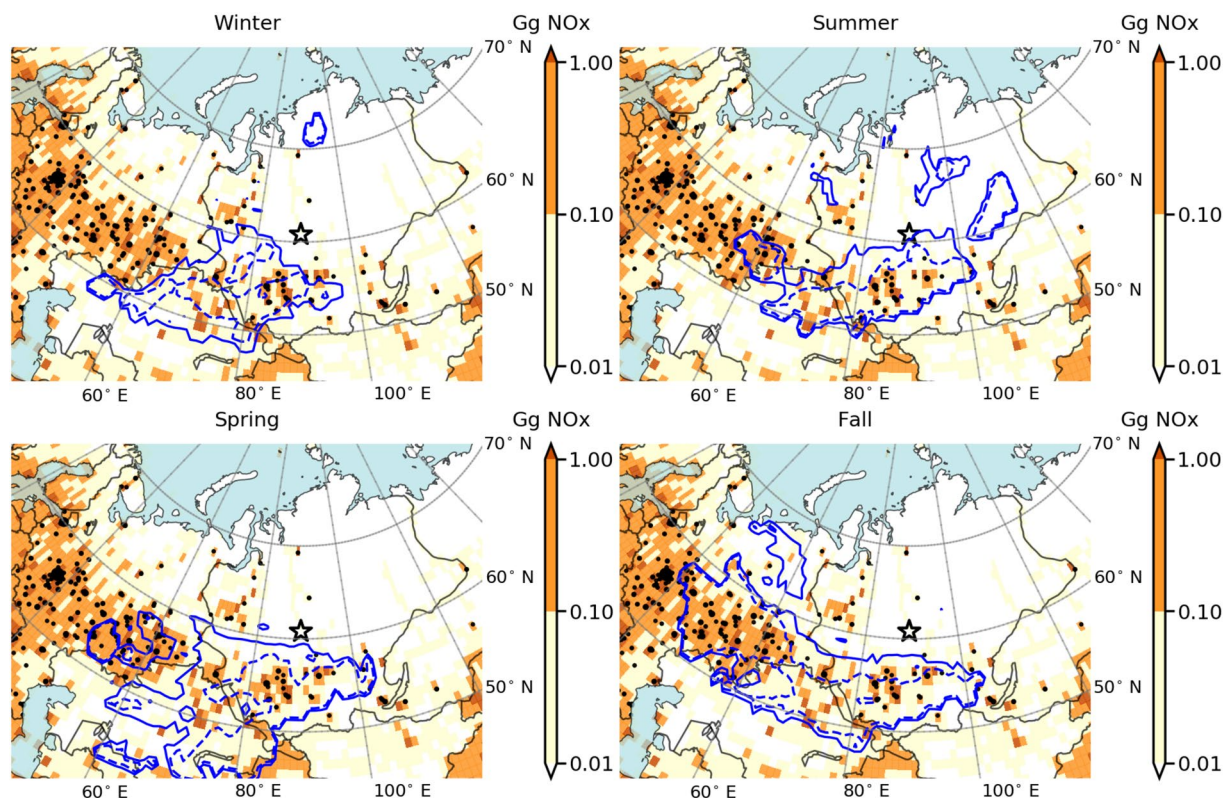


**Figure 6.** The regions of high potential contribution to high  $\text{NO}_x$  at ZOTTO outlined with the contours of CP values 0.25 (solid line) and 0.50 (dashed line) (see Section 2.4); color bar shows the monthly average anthropogenic  $\text{NO}_x$  emissions ( $10^9 \text{ g NO}_x$ ) for each season over years 2007–2014.

ure 6. This is consistent with the observed seasonal variations of wildfire activity in the region, which exhibits a marked latitudinal shift from the southern areas in spring and autumn to the central and northern parts of Siberia ( $>60^\circ\text{N}$ ) in summer, following seasonal cycles of solar radiation and precipitation in the region (Ponomarev et al., 2016; Vasileva et al., 2010). Noting the high variability of wildfire emissions in space and time and the associated uncertainties in the trajectory analysis, we consider the above spatial discrimination of the fire-related  $\text{NO}_x$  sources as strong evidence for the overall consistency of all the assumptions underlying the CP-based approach.

One can also see that the clean air originates mostly from continental areas with a minor anthropogenic load (*remote areas* thereafter) in the mid-to-high latitude belt  $55^\circ\text{--}70^\circ\text{N}$  (Figure 7), thus showing a distinct separation between the origins of clean and polluted air masses. According to the measured  $\text{NO}_x$  variations, we then associate clean and polluted air at ZOTTO with CB, that is, not subjected to the impact of regional pollution sources, and REI air masses, to emphasize the regional extent of the derived estimates. Alternatively, one could retain only the grid cells with statistically significant CP values according to the binomial test (Vasconcelos et al., 1996) or employ a more sophisticated Kolmogorov–Zurbenko low-pass filter (for details, see Vasileva et al., 2011 and references therein) for the  $\text{NO}_x$  data to constrain the specified time range of the synoptic fluctuations, with the main quantitative results of our analysis remaining essentially unchanged. Hence, the CP-based approach employed for the ZOTTO data analysis does provide robust constraints on the source area of  $\text{NO}_x$  for the site, and the ranges of the observed  $\text{NO}_x$  levels that are representative of clean and regionally polluted conditions.

### 3.5. Seasonal Variations of Ozone in Continental Versus NH Midlatitude Baseline Air

By separating the air masses into CB and REI categories according to the measured  $\text{NO}_x$  variations, the overall effect of regional pollution sources on the ozone levels at ZOTTO can be quantified on a monthly

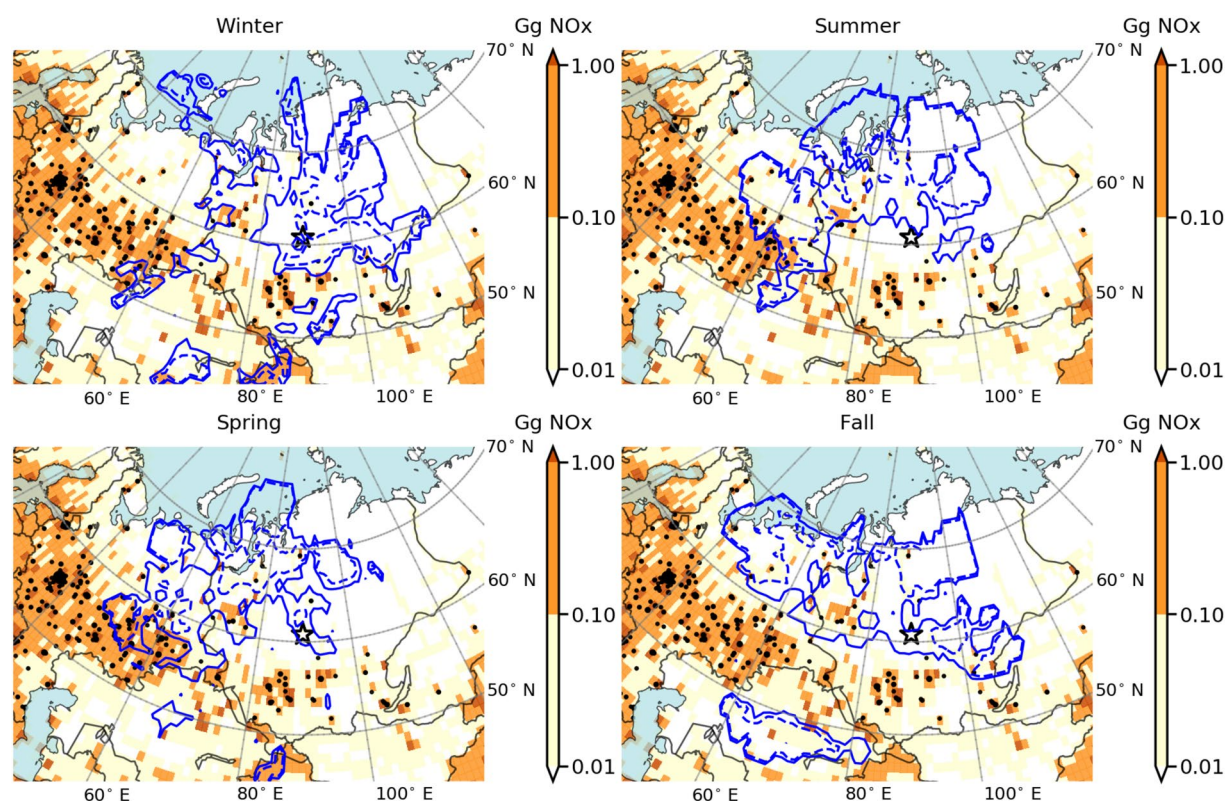


**Figure 7.** As Figure 6 but with the CP contours outlining the regions of the most likely contribution to low  $\text{NO}_x$  at ZOTTO.

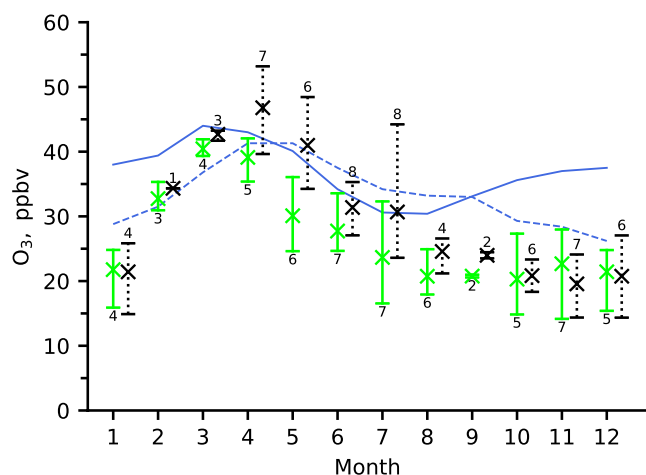


**Figure 8.** Seasonal dependence of daytime (12:00–18:00)  $\text{O}_3$  mixing ratios at ZOTTO for CB (green) and REI (black) air masses (the 2007–2014 averages and min–max of monthly means); labels give the number of monthly ozone data used for calculating statistics. The  $\text{O}_3$  data points for REI air are offset horizontally by 0.3 along the abscissa for better visibility. For comparison, the 1987–2012 monthly mean  $\text{O}_3$  levels in clean (solid blue line) and regionally polluted (dashed blue line) air masses arriving from the European continent at the Mace Head station ( $53^\circ\text{N}$ ,  $10^\circ\text{E}$ , 25 m asl) are provided according to Derwent et al. (2013).

basis. Mean, minimum, and maximum monthly ozone levels have been estimated separately for CB and REI air based on the respective subsets of days from the month associated with clean and polluted conditions, correspondingly. The derived monthly ozone data were used to calculate the corresponding average and variability (min–max) interval for each month and air mass (Figure 8) for the years 2007–2014. Since each of the CB and REI data subsets involves only a quarter of the original daily ozone data for each season, the monthly mean is estimated using approximately seven daily ozone values on average. Also, significant gaps in the original data affect the confidence of the derived statistics for months with low data coverage. Yet, the results obtained through separating ozone data into clean and polluted categories according to the median of daily  $[\text{NO}_x']$  values (so that the whole  $\text{O}_3$  dataset is involved in the statistic calculations) do not show much difference from those shown in Figure 8. This supports the general notion that the derived average seasonal cycles do provide a quantitative basis for comparing ozone levels in different air masses, whereas the observed interannual variability of monthly ozone values represents only some part of the total climatic variability of ozone at the site.

For comparison, we reproduce in Figure 8 the seasonal cycles of monthly average ozone at the Mace Head (Ireland) atmospheric research station associated with clean (“baseline” in the author’s notation) air masses, transported mainly from central North Atlantic, and the polluted air, transported from the western part of the European continent (“European regionally polluted air”), as reported by Derwent et al. (2013). Below, we



refer to the European origin of the polluted air measured at Mace Head as Western Europe, yet being aware of the site-specific pattern of the air transport climatology. As far as the amplitude of the diurnal cycle of ozone at Mace Head is low throughout the year, reaching its maximum of an order of a few ppbv in summer months (Tripathi et al., 2012), these measurements are probably representative of average ozone values within the planetary boundary layer under well-mixed conditions. This feature allows for direct comparison with the afternoon ozone data at the ZOTTO site, where ozone mixing ratios are subjected to strong diurnal variations in spring and summer (Figure 3). The Mace Head baseline ozone data have been identified previously as representative of the “Northern Hemisphere midlatitude baseline” (NHMLB) air to identify the European continent as a net source or sink for the tropospheric ozone on a hemispheric scale (Derwent et al., 1998, 2013). Here we employ the ozone data at Mace Head and ZOTTO for quantitative comparison of NHMLB and continental (CB and REI) air and the assessment of the importance of Siberia for the midlatitude ozone budget.

One can see from Figure 8 that ozone in NHMLB and CB air masses reaches its annual maximum in March, with the 2007–2014 monthly average mixing ratio of 40.5 ppbv at ZOTTO and about 44 ppbv at Mace Head. The observed marked similarity in the absolute value and time of the ozone maximum for clean air at the two sites (as well as in TROICA campaigns discussed above), which are highly different in meteorological conditions and the origins of the measured air masses, strongly supported the earlier conclusion on the polar front reservoir mechanism (Derwent et al., 1998; Monks, 2000; Penkett & Brice, 1986; Vingarzan, 2004) as a common source for the early springtime ozone maximum both in the maritime and CBL in the Northern Hemisphere midlatitudes.

Ozone levels in the European regionally polluted air exceed those in NHMLB air from May to August when the European region was found to represent a net source of tropospheric ozone on the hemispheric scale (Derwent et al., 1998). A similar seasonal pattern of the enhanced ozone levels in the polluted air is clearly seen for the ZOTTO site from February to October when ozone levels in REI air exceed those in CB air by up to 11 ppbv on average in May. Hence, air pollutant emissions in Siberia provide a net source for ozone in CBL over central North Eurasia for an appreciably longer period of year compared to the similar effect of emissions for the region of Western Europe. The prolonged period of net photochemical ozone production in Siberia can be explained at least partially by substantially weaker anthropogenic  $\text{NO}_x$  emissions in the region compared to those in Western Europe (Moiseenko et al., 2018) and proportionally lower  $\text{NO}_x$  levels in the CBL. During late winter and early spring under low solar radiation, the efficiency of photochemical ozone production through the chemical chain reactions involving  $\text{NO}_x$  is expected to be low under strongly limited tropospheric hydroxyl abundance, so that titration of the ozone by reaction with anthropogenic  $\text{NO}_x$  still contributes to ozone destruction at a rate that is proportional to the regional  $\text{NO}_x$  supply. Hence, low  $\text{NO}_x$  levels in the CBL are expected to result both in higher efficiency of ozone production per  $\text{NO}_x$  molecule consumed (S. C. Liu et al., 1987) and less importance of ozone sink via the chemical reaction with  $\text{NO}_x$ , resulting in net positive photochemical ozone production in the Siberia region. This is contrasted to Mace Head and other rural monitoring sites in northwest Europe where the destruction of ozone through reaction with  $\text{NO}_x$  and other pollutants may still dominate over ozone production owing to the proximity of strong regional sources of ozone precursors (Solberg et al., 1997). The earlier onset of the period of net positive photochemical ozone production in Siberia, accompanied by ozone accumulation in CBL, explains the observed higher (by up to 6 ppb in April, see Figure 8) multi-year average ozone levels in REI air in late winter and early spring compared to the respective ozone levels in polluted air masses coming from western Europe to Mace Head.

In Figure 8 one can see that multi-year average ozone levels in REI air exceed those in NHMLB air in April to May by 3–5 ppbv. The regional pollutant emissions in Siberia provide then a seasonal source for ozone in the midlatitude planetary boundary layer on the hemispheric scale in these months. Additionally, high ozone levels are frequently observed in individual months of the summer season in years when persistent anticyclonic weather conditions result in high daytime air temperatures and solar radiation. Correspondingly, the multi-year average ozone levels in REI air are seen to be close to ozone values in NHMLB air in June and July, as the ozone statistics for these months are influenced by high monthly ozone values in individual years of the observation period. In months of enhanced regional ozone production from April to July, for which the highest difference between ozone abundance in REI and CB air is observed, monthly ozone levels for REI air

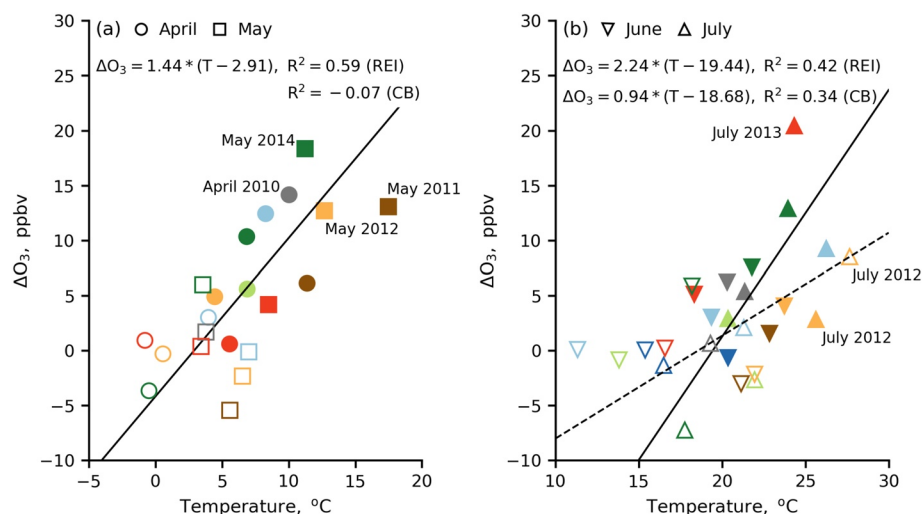


**Figure 9.** Difference between monthly daytime ozone value for the given air mass and the corresponding 2007–2014 average ozone level for CB air versus temperature in April to May (a) and June to July (b) for CB (open) and REI (filled) air at ZOTTO. The lines give the linear, two-sided regression fit to the REI (solid) and CB (dashed) ozone data.

exceed NHMLB ozone levels in 13 of total 26 months of observations at ZOTTO, which suggests the Siberia region as a net source for ozone in hot summer seasons. This finding of the present study is in contrast to the previous studies (Engvall-Stjernberg et al., 2012; Pochanart et al., 2003; Wild et al., 2004) considering Siberia as the net ozone sink throughout the year.

The temperature-dependent regime of ozone photochemical production in REI air from regional ozone precursors is clearly seen in Figure 9 which shows the 1.4 and 2.2 ppbv increase in daytime ozone per °C for REI air in April to May and June to July, correspondingly, on a monthly basis. This can be attributed to the combined effect of temperature-enhanced emissions of highly reactive BVOCs (BVOCs), soil emissions of NO<sub>x</sub>, as well as to the increased odd hydrogen production rate (through its dependence on UV radiation) from photolysis of ozone and other species (Bowman & Seinfeld, 1994; Pusede et al., 2014; Romer et al., 2018; Trainer, Hsieh et al., 1987; Trainer, Williams et al., 1987) on the daytime surface ozone levels. Although reactions of ozone with monoterpenes and other BVOCs provide a significant part of the overall ozone in-canopy sink in a forested environment (Wolfe et al., 2011), the present results strongly suggest an important role of the regional emissions of BVOCs in the photochemical ozone production under the measured NO<sub>x</sub> levels. A potentially significant role of biogenic emissions for the regional ozone balance has been suggested previously by the sensitivity simulations using the GEOS-Chem chemical transport model for conditions with and without BVOC and anthropogenic NO<sub>x</sub> emissions in Siberia (49°–75°N, 60°–120°E; Moiseenko et al., 2018, see also Section 3.5). The exponential increase in the biogenic isoprene and total VOCs mixing ratios with temperature have been observed for clean and regionally polluted air in the TROICA measurement campaign in summer 2012 (Berezina et al., 2019), with the highest mixing ratios of isoprene and monoterpenes of 2–2.5 ppbv and 3–9 ppbv, correspondingly, observed under high temperatures (>28°C) and solar radiation (E. V. Berezina, personal communication). The observed temporal variations in the daytime ozone levels along the TROICA route correspond well to the variations in isoprene and monoterpenes, which likely reflects the influence of BVOCs on the ozone formation.

The significant positive correlation of ozone with temperature ( $R^2 = 0.34$ ) is seen in summer not only for the polluted REI air but for the clean CB air as well (Figure 9b). It can be likely attributed to the pure effect of the biogenic emissions of ozone precursors in clean CBL over the remote areas of Siberia. The calculations with the default soil NO<sub>x</sub> emission scheme of Hudman et al. (2012) adapted in the GEOS-Chem model give the domain-total annual emissions of 0.28–0.36 Tg NO<sub>x</sub>. This is comparable to the 0.6 Tg of anthropogenic and 0.08–0.18 Tg of wildfire NO<sub>x</sub> emissions in the region (Moiseenko et al., 2018), thus suggesting an important role of biogenic NO<sub>x</sub> in the regional ozone photochemistry. The observed difference between the O<sub>3</sub>–temper-



ature slope rates in REI and CB air in summer (2.2 vs. 0.9 ppbv O<sub>3</sub> per °C) then quantifies a direct effect of anthropogenic and fire-emitted NO<sub>x</sub> on the net ozone production in addition to the temperature-controlled NO<sub>x</sub> emissions from biogenic sources. Statistically significant dependence of the CB ozone on temperature is absent for the springtime data (Figure 9a) due to low seasonal temperatures and the associated biogenic emissions. In the study of Doherty et al. (2013), the sensitivity simulations with the STOC-HadAM3 coupled climate-chemistry model were performed to quantify the impact of different chemical processes, influenced by climate change, on the surface O<sub>3</sub> levels. According to their study, a 3°C increase in temperature applied to the isoprene emissions alone would increase surface ozone by 0.5–1 ppbv in the North Eurasia midlatitudes, resulting in the equivalent O<sub>3</sub>–temperature slope rate of 0.17–0.3 ppbv per °C. This contributes a significant fraction of the 0.9 ppbv O<sub>3</sub> per °C ozone response value for the clean air shown in Figure 9b, with the remaining part of the total O<sub>3</sub>–temperature correlation likely attributed to the temperature-enhanced soil NO<sub>x</sub> emissions and chemistry (Pusede et al., 2014; Romer et al., 2018; Schindlbacher, 2004). The results of the present study thus strongly suggest that interactions between the regional anthropogenic and wildfire pollutants and BVOCs must be better quantified for better assessment of photochemical ozone formation in remote CBL over Siberia.

Compared to the more straightforward ozone–temperature relationship, the impact of wildfires on the measured ozone levels seems to be more complex. Thus, suppressed ozone levels are often observed in a photochemically young air, while net ozone production is reported in field studies on a later stage of plume evolution (Jaffe & Wigder, 2012; Tanimoto et al., 2008). Both the effects are distinguished in ZOTTO data. Figure 9 shows a negative difference between monthly ozone mixing ratios for REI and CB air of about 6 ppbv in July 2012, a period of strong wildfires in central Siberia and directly around ZOTTO. This is contrasted to strong wildfires in northern and central Siberia in July 2013 resulting in a monthly ozone level of 45 ppbv, the highest mean ozone value over the 2007–2014 summer seasons. The ozone value in July 2013 (Figure 9b, red triangle) is 20 and 14 ppbv higher compared to the multi-year average ozone levels in CB and HNMLB air, correspondingly. A more straightforward dependence of ozone on distant wildfires in southern Siberia and Northern Kazakhstan is found in spring. Figure 9a shows the highest positive differences between ozone values for REI and CB air of 13–18 ppbv for the months of severe wildfires (April 2010, May 2011, 2012, and 2014). These are also the months of the highest springtime ozone values of 53 ppbv in April and up to 48 ppbv in May over the measurement period. We can finally conclude, based on the present data, that severe wildfires in southern and central Siberia provide a net source for the midlatitude ozone on the regional and global scales in a period from spring to early summer under favorable weather conditions (see also Jaffe et al., 2004; Johnson et al., 2021; Lapina, 2009 and references therein).

The seasonal cycle of the baseline ozone at Mace Head has a distinct minimum in July to August, reflecting the transition from positive net photochemical ozone production in spring to its destruction in summer within the maritime boundary layer (Derwent et al., 1998). This is contrasted to the average CB ozone at ZOTTO, as well as ozone in the European polluted air at Mace Head, which both show a monotonic decrease of monthly O<sub>3</sub> mixing ratios throughout late spring and summer typical for other midlatitude weakly polluted sites (Katragkou et al., 2015; Monks, 2000; Solberg et al., 1997) where ozone reaches its annual minimum in late summer and early autumn. The observed shift in the seasonal ozone minimum in CB air to the late autumn compared to the summertime ozone minimum in clean air for Mace Head evidences for a weak persisting photochemical production of ozone during summer months in remote CBL owing to biogenic and biomass burning emissions of ozone precursors which maintain baseline NO<sub>x</sub> and VOC at levels high enough for the net positive ozone production in clean air. Yet, observations at ZOTTO show systematically lower ozone abundance in CB air compared to that in HNMLB air, by ~5–15 ppbv from spring to late autumn and by up to 18 ppbv in winter, reflecting the first-order effect of the surface deposition process on the ozone balance in the region (Engvall-Stjernberg et al., 2012; Hirdman et al., 2010). We then conclude finally that the regions of remote North Eurasia that we associate with the CB air masses represent a net sink for ozone on a global scale throughout the year, in close agreement with some previous studies (Engvall-Stjernberg et al., 2012; Paris et al., 2010).

#### 4. Conclusions

The source–receptor relationship of  $O_3$  and  $NO_x$  for ZOTTO, a remote site in central Siberia, has been examined for the observation period from March 2007 till December 2014 using the CP Function analysis coupled with a back-trajectory model. Daily ensembles of trajectories were assigned to the  $NO_x$  data, and the origins of polluted (REI) and clean (CB) air masses carrying high and low  $NO_x$  to ZOTTO, correspondingly, were spatially localized. The model-predicted source area of pollutant emissions affecting the ZOTTO site is clearly associated with industrial regions of western Siberia and southern Ural Mountains, whereas CB air originates mainly from remote areas of North Eurasia including north of European Russia, central and northern Siberia within the 55°–70°N latitude belt. Additionally, biomass burning  $NO_x$  emissions, of which the major part is emitted from wildfires in boreal forests of the southern and central Siberia and steppe fires of Northern Kazakhstan, contribute to the regional  $NO_x$  input in severe fire seasons. Monthly ozone levels for REI air are found to be higher by 7 ppbv on average in February to October and lower by 2 ppbv from November to January than those for CB air, reflecting the seasonal change in ozone photochemistry from net photochemical ozone production during most of the year to its destruction in late autumn and early winter in the regionally polluted air. At present, the derived seasonal cycle of the CB ozone provides the most complete determination of the near-surface ozone climatology for the remote central North Eurasia at the given latitude and elevation.

The ozone seasonal cycles for clean and polluted air at ZOTTO and Mace Head (Ireland), a remote monitoring site measuring ozone levels at the western inflow boundary of the continent, were compared to assess the relative importance of central North Eurasia as a net source or sink of the tropospheric ozone on the regional and global scales. The ozone seasonal maxima at both the sites are observed in March and April for clean and regionally polluted air, correspondingly. This evidences of a common hemispheric-wide source for the springtime ozone maxima at the two sites, upon which a regional effect of ozone precursor emissions is superimposed. Essentially, the period of net photochemical ozone production in the regionally polluted air at ZOTTO is observed for a substantially longer period (from February to October) compared to the similar period at Mace Head lasting from May to August.

Our results agree with the general conclusion of previous studies (Engvall-Stjernberg et al., 2012; Paris et al., 2010; Thorp et al., 2020) that surface ozone in the region of observations is controlled mainly by the balance between regional anthropogenic emissions and seasonally varying processes of atmospheric transport and surface deposition. Consequently, the ozone levels in CB air are found to be substantially less than those for clean air masses at Mace Head throughout the year. The remote areas of North Eurasia then represent a sink for ozone in the boundary layer throughout the year on the hemispheric scale.

In late spring (April–May), regional anthropogenic and wildfire emissions provide a seasonal source for ozone in CBL over Siberia, resulting in ozone levels well exceeding those observed in the CB and the NHMLB air according to the Mace Head data. In summer, hot weather conditions accompanied by high UV radiation are favorable for enhanced photochemical ozone production in REI air from the regional ozone precursors, with monthly ozone levels in polluted air greatly exceeding those in CB and NHMLB air masses. Throughout the most photochemically active season from April to July, the highest ozone levels are observed in years of strongest fire activity, where the combined effect of anthropogenic and temperature-enhanced biogenic emissions of VOCs and  $NO_x$  is amplified by wildfire emissions of ozone precursors. Consequently, in individual years of persisting anticyclonic weather and accompanying strong fire activity, the regions of southern and central Siberia represent a net source for ozone on the hemispheric scale during summer months as well. This finding of the present investigation is in contrast with the previous studies (Engvall-Stjernberg et al., 2012; Pochanart et al., 2003; Wild et al., 2004) considering Siberia as a net ozone sink throughout the year. The potential roles of BVOC and anthropogenic ozone precursors in the regional photochemistry should be thoroughly studied for a better assessment of the anthropogenic impact on the regional ecosystems and air quality, as well as projections of future ozone changes driven by climate change.

#### Conflict of Interest

The authors declare no conflicts of interest relevant to this study.

## Data Availability Statement

We thank the Joint Research Center of the European Commission for the EDGARv4.3.2 emissions database (<http://edgar.jrc.ec.europa.eu/overview.php?v=432&SECURE=123>) used in this study ([https://data.europa.eu/doi/10.2904/JRC\\_DATASET\\_EDGAR](https://data.europa.eu/doi/10.2904/JRC_DATASET_EDGAR)), as well as the research team of the <http://globalfiredata.org> for the GFEDv4.1s (<https://doi.org/10.3334/ORNLDAAAC/1293>) wildfire emissions database. We kindly thank the ZOTTO consortium for the ozone data (<https://join.fz-juelich.de/access/db/>; <http://doi.org/10.17616/R3FZ0G>).

## Acknowledgments

The authors thank the colleagues from the Meteorological Observatory of the M. V. Lomonosov Moscow State University for the meteorological information. The study was funded by the Ministry of Science and Higher Education of the Russian Federation under agreement No 075-15-2020-776.

## References

- Arnold, S. R., Lombardozzi, D., Lamarque, J. F., Richardson, T., Emmons, L. K., Tilmes, S., et al. (2018). Simulated global climate response to tropospheric ozone-induced changes in plant transpiration. *Geophysical Research Letters*, 45(23), 13070–13079. <https://doi.org/10.1029/2018GL079938>
- Ashbaugh, L. L., Malm, W. C., & Sadeh, W. D. (1985). A residence time probability analysis of sulfur concentrations at Grand Canyon National Park. *Atmospheric Environment*, 19, 1263–1270. [https://doi.org/10.1016/0004-6981\(85\)90256-2](https://doi.org/10.1016/0004-6981(85)90256-2)
- Atkinson, R. W., Butland, B. K., Dimitroulopoulou, C., Heal, M. R., Stedman, J. R., Carslaw, N., et al. (2016). Long-term exposure to ambient ozone and mortality: A quantitative systematic review and meta-analysis of evidence from cohort studies. *BMJ Open*, 6(2), 1–10. <https://doi.org/10.1136/bmjopen-2015-009493>
- Berezina, E., Moiseenko, K., Skorokhod, A., Elansky, N., Belikov, I., & Pankratova, N. (2019). Isoprene and monoterpenes over Russia and their impacts in tropospheric ozone formation. *Geography, Environment, Sustainability*, 12(1), 63–74. <https://doi.org/10.24057/2071-9388-2017-24>
- Bowman, F. M., & Seinfeld, J. H. (1994). Ozone productivity of atmospheric organics. *Journal of Geophysical Research*, 99(D3), 5309–5324. <https://doi.org/10.1029/93JD03400>
- Browne, E. C., & Cohen, R. C. (2012). Effects of biogenic nitrate chemistry on the NO<sub>x</sub> lifetime in remote continental regions. *Atmospheric Chemistry and Physics*, 12, 11917–11932. <https://doi.org/10.5194/acp-12-11917-2012>
- Cailleret, M., Ferretti, M., Gessler, A., Rigling, A., & Schaub, M. (2018). Ozone effects on European forest growth—Toward an integrative approach. *Journal of Ecology*, 106, 1377–1389. <https://doi.org/10.1111/1365-2745.12941>
- Chan, E., & Vet, R. J. (2010). Baseline levels and trends of ground level ozone in Canada and the United States. *Atmospheric Chemistry and Physics*, 10, 8629–8647. <https://doi.org/10.5194/acp-10-8629-2010>
- Chi, X., Winderlich, J., Mayer, J.-C., Panov, A. V., Heimann, M., Birmili, W., et al. (2013). Long-term measurements of aerosol and carbon monoxide at the ZOTTO tall tower to characterize polluted and pristine air in the Siberian taiga. *Atmospheric Chemistry and Physics*, 13, 12271–12298. <https://doi.org/10.5194/acp-13-12271-2013>
- Crutzen, P. J., Elansky, N. F., Hahn, M., Golitsyn, G. S., Brenninkmeijer, C. A. M., Scharffe, D., et al. (1998). Trace gas measurements between Moscow and Vladivostok using the Trans-Siberian Railroad. *Journal of Atmospheric Chemistry*, 29, 179–194. <https://doi.org/10.1023/A:1005848202970>
- Derwent, R. G., Manning, A. J., Simmonds, P. G., Spain, T. G., & O'Doherty, S. (2013). Analysis and interpretation of 25 years of ozone observations at the Mace Head Atmospheric Research Station on the Atlantic Ocean coast of Ireland from 1987 to 2012. *Atmospheric Environment*, 80, 361–368. <https://doi.org/10.1016/j.atmosenv.2013.08.003>
- Derwent, R. G., Simmonds, P. G., Seuring, S., & Dimmer, C. (1998). Observation and interpretation of the seasonal cycles in the surface concentrations of ozone and carbon monoxide at Mace Head, Ireland from 1990 to 1994. *Atmospheric Environment*, 32(2), 145–157. [https://doi.org/10.1016/s1352-2310\(97\)00338-5](https://doi.org/10.1016/s1352-2310(97)00338-5)
- Doherty, R. M., Wild, O., Shindell, D. T., Zeng, G., MacKenzie, I. A., Collins, W. J., et al. (2013). Impacts of climate change on surface ozone and intercontinental ozone pollution: A multi-model study. *Journal of Geophysical Research*, 118, 3744–3763. <https://doi.org/10.1002/jgrd.50266>
- Elansky, N. F. (Ed.). (2009). *Atmospheric composition observations over northern Eurasia using the mobile laboratory: TROICA experiments* (p. 84). International Science and Technology Center.
- Eneroth, K., Kjellstrom, E., & Holmen, K. (2003). Interannual and seasonal variations in transport to a measuring site in western Siberia and their impact on the observed atmospheric CO<sub>2</sub> mixing ratio. *Journal of Geophysical Research*, 108(D21), 4660. <https://doi.org/10.1029/2002JD002730>
- Engvall-Stjernberg, A.-C., Skorokhod, A. I., Elansky, N. F., Paris, J.-D., Nédélec, P., & Stohl, A. (2012). Low surface ozone in Siberia. *Tellus B: Chemical and Physical Meteorology*, 64, 11607. <https://doi.org/10.3402/tellusb.v64i0.11607>
- Felzer, B., Reilly, J., Melillo, J., Kicklighter, D., Sarofim, M., Wang, C., et al. (2005). Future effects of ozone on carbon sequestration and climate change policy using a global biogeochemical model. *Climatic Change*, 73, 345–373. <https://doi.org/10.1007/s10584-005-6776-4>
- Fuhrer, J. (2009). Ozone risk for crops and pastures in present and future climates. *Naturwissenschaften*, 96(2), 173–194. <https://doi.org/10.1007/s00114-008-0468-7>
- Heimann, M., Schulze, E. D., Winderlich, J., Andreae, M. O., Chi, X., Gerbig, C., et al. (2014). The Zotino Tall Tower Observatory (Zotto): Quantifying large scale biogeochemical changes in Central Siberia. *Nova Acta Leopoldina*, 117(399), 51–64.
- Hirdman, D., Sodermann, H., Eckhardt, S., Burkhardt, J. F., Jefferson, A., Mefford, T., et al. (2010). Source identification of short-lived air pollutants in the Arctic using statistical analysis of measurement data and particle dispersion model output. *Atmospheric Chemistry and Physics*, 10, 669–693. <https://doi.org/10.5194/acp-10-669-2010>
- Hollaway, M. J., Arnold, S. R., Challinor, A. J., & Emberson, L. D. (2012). Intercontinental trans-boundary contributions to ozone-induced crop yield losses in the Northern Hemisphere. *Biogeosciences*, 9(1), 271–292. <https://doi.org/10.5194/bg-9-271-2012>
- Hudman, R. C., Moore, N. E., Mebust, A. K., Martin, R. V., Russell, A. R., Valin, L. C., & Cohen, R. C. (2012). Steps toward a mechanistic model of global soil nitric oxide emissions: Implementation and space based-constraints. *Atmospheric Chemistry and Physics*, 12, 7779–7795. <https://doi.org/10.5194/acp-12-7779-2012>
- Jaffe, D. A., Bertschi, I., Jaeglé, L., Novelli, P., Reid, J. S., Tanimoto, H., et al. (2004). Long-range transport of Siberian biomass burning emissions and impact on surface ozone in western North America. *Geophysical Research Letters*, 31(16), 6–9. <https://doi.org/10.1029/2004GL020093>

- Jaffe, D. A., & Wigder, N. L. (2012). Ozone production from wildfires: A critical review. *Atmospheric Environment*, 51, 1–10. <https://doi.org/10.1016/j.atmosenv.2011.11.063>
- Janssens-Maenhout, G., Crippa, M., Guizzardi, D., Muntean, M., Schaaf, E., Dentener, F., et al. (2019). EDGAR v4.3.2 Global Atlas of the three major greenhouse gas emissions for the period 1970–2012. *Earth System Science Data*, 11(3), 959–1002. <https://doi.org/10.5194/essd-11-959-2019>
- Johnson, M. S., Strawbridge, K., Knowland, K. E., Keller, C., & Travis, M. (2021). Long-range transport of Siberian biomass burning emissions to North America during FIREX-AQ. *Atmospheric Environment*, 252(52–63), 118241. <https://doi.org/10.1016/j.atmosenv.2021.118241>
- Katragkou, E., Zanis, P., Tsikerdekis, A., Kapsomenakis, J., Melas, D., Eskes, H., et al. (2015). Evaluation of near-surface ozone over Europe from the MACC reanalysis. *Geoscientific Model Development*, 8, 2299–2314. <https://doi.org/10.5194/gmd-8-2299-2015>
- Kenagy, H. S., Sparks, T. L., Ebben, C. J., Wooldridge, P. J., Lopez-Hilfiker, F. D., Lee, B. H., et al. (2018). NO<sub>x</sub> lifetime and NO<sub>y</sub> partitioning during winter. *Journal of Geophysical Research*, 123, 9813–9827. <https://doi.org/10.1029/2018JD028736>
- Kleinman, L. I., Daum, P. H., Lee, J. H., Lee, Y., Nunnermacker, L. J., Stephen, R. S., et al. (1997). Dependence of ozone production on NO and hydrocarbons in the troposphere. *Geophysical Research Letters*, 101(18), 2299–2302. <https://doi.org/10.1029/97GL02279>
- Kotelnikov, S. N., Stepanov, E. V., & Ivashkin, V. T. (2017). Ozone concentration in the ground atmosphere and morbidity during extreme heat in the summer of 2010. *Doklady Biological Sciences*, 473(1), 64–68. <https://doi.org/10.1134/S0012496617020107>
- Kozlova, E. A., & Manning, A. C. (2009). Methodology and calibration for continuous measurements of biogeochemical trace gas and O<sub>2</sub> concentrations from a 300-m tall tower in central Siberia. *Atmospheric Measurement Techniques*, 2(1), 205–220. <https://doi.org/10.5194/amt-2-205-2009>
- Lapina, K. (2009). *Boreal forest fire impacts on lower troposphere carbon monoxide and ozone levels at the regional to hemispheric scales* (Doctoral dissertation). Michigan Technological University. Retrieved from [Digital Commons—Michigan Technology]. <https://doi.org/10.37099/mtu.dc.ets/712>
- Lin, X., Trainer, M., & Liu, S. C. (1988). On the nonlinearity of the tropospheric ozone production. *Journal of Geophysical Research*, 93(D12), 15879–15888. <https://doi.org/10.1029/JD093iD12p15879>
- Liu, F., Beirle, S., Zhang, Q., Dörner, S., He, K., & Wagner, T. (2016). NO<sub>x</sub> lifetimes and emissions of cities and power plants in polluted background estimated by satellite observations. *Atmospheric Chemistry and Physics*, 16, 5283–5298. <https://doi.org/10.5194/acp-16-5283-2016>
- Liu, S. C., Trainer, M., Fehsenfeld, F. C., Parrish, D. D., Williams, E. J., Fahey, D. W., et al. (1987). Ozone production in the rural troposphere and the implications for regional and global ozone distributions. *Journal of Geophysical Research*, 92, 4191–4207. <https://doi.org/10.1029/JD092iD04p04191>
- Lloyd, J., Langenfelds, R. L., Francey, R. J., Gloor, M., Tchekakova, N. M., Zolotoukhine, D., et al. (2002). A trace-gas climatology above Zotino, central Siberia. *Tellus B: Chemical and Physical Meteorology*, 54(5), 749–767. <https://doi.org/10.3402/tellusb.v54i5.16726>
- Logan, J. A. (1985). Tropospheric ozone: Seasonal behavior, trends and anthropogenic influence. *Journal of Geophysical Research*, 90(10), 463–482. <https://doi.org/10.1029/JD090iD06p10463>
- Logan, J. A. (1989). Ozone in rural areas of the United States. *Journal of Geophysical Research*, 94(D6), 8511–8532. <https://doi.org/10.1029/JD094iD06p08511>
- Mikhailov, E. F., Mironova, S., Mironov, G., Vlasenko, S., Panov, A., Chi, X., et al. (2017). Long-term measurements (2010–2014) of carbonaceous aerosol and carbon monoxide at the Zotino Tall Tower Observatory (ZOTTO) in central Siberia. *Atmospheric Chemistry and Physics*, 17(23), 14365–14392. <https://doi.org/10.5194/acp-17-14365-2017>
- Mills, G., Buse, A., Gimeno, B., Bermejo, V., Holland, M., Emberson, L., & Pleijel, H. (2007). A synthesis of AOT40-based response functions and critical levels of ozone for agricultural and horticultural crops. *Atmospheric Environment*, 41, 2630–2643. <https://doi.org/10.1016/j.atmosenv.2006.11.016>
- Mills, G., Hayes, F., Simpson, D., Emberson, L., Norris, D., Harmens, H., & Büker, P. (2011). Evidence of widespread effects of ozone on crops and (semi-)natural vegetation in Europe (1990–2006) in relation to AOT40- and flux-based risk maps. *Global Change Biology*, 17(1), 592–613. <https://doi.org/10.1111/j.1365-2486.2010.02217.x>
- Moiseenko, K. B., Berezina, E. V., Vasileva, A. V., Shtabkin, Y. A., Skorokhod, A. I., Elanskii, N. F., & Belikov, I. B. (2019). The NO<sub>x</sub>-limiting regime of photochemical ozone generation in a weakly polluted convective boundary layer: Observations at the ZOTTO tall tower observatory in central Siberia, 2007–2015. *Doklady Earth Sciences*, 487(2), 981–985. <https://doi.org/10.1134/S1028334X19080282>
- Moiseenko, K. B., Shtabkin, Y. A., Berezina, E. V., & Skorokhod, A. I. (2018). Regional photochemical surface-ozone sources in Europe and Western Siberia. *Izvestiya, Atmospheric and Oceanic Physics*, 54(6), 545–557. <https://doi.org/10.1134/S0001433818060105>
- Monks, P. S. (2000). A review of the observations and origins of the spring ozone maximum. *Atmospheric Environment*, 34(21), 3545–3561. [https://doi.org/10.1016/S1352-2310\(00\)00129-1](https://doi.org/10.1016/S1352-2310(00)00129-1)
- Mu, M., Randerson, J. T., van der Werf, G. R., Giglio, L., Kasibhatla, P., Morton, D., et al. (2011). Daily and 3-hourly variability in global fire emissions and consequences for atmospheric model predictions of carbon monoxide. *Journal of Geophysical Research*, 116(D24). <https://doi.org/10.1029/2011JD016245>
- Myhre, G., Shindell, D., Bréon, F.-M., Collins, W., Fuglestad, J., Huang, J., et al. (2013). *Anthropogenic and natural radiative forcing. Climate change 2013: The physical science basis. Contribution of working group I to the fifth assessment report of the Intergovernmental Panel on climate change*. Cambridge University Press.
- Oltmans, S. J. (1981). Surface ozone measurements in clean air. *Journal of Geophysical Research*, 86(C2), 1174–1180. <https://doi.org/10.1029/JC086iC02p01174>
- Paris, J.-D., Ciais, P., Nédélec, P., Ramonet, M., Belan, B. D., Arshinov, M., et al. (2008). The YAKAEROSIB transcontinental aircraft campaigns: New insights on the transport of CO<sub>2</sub>, CO and O<sub>3</sub> across Siberia and in the Northern Hemisphere. *Tellus B: Chemical and Physical Meteorology*, 60(4), 551–568. <https://doi.org/10.1111/j.1600-0889.2008.00369.x>
- Paris, J.-D., Stohl, A., Ciais, P., Nédélec, P., Belan, B. D., Arshinov, M., et al. (2010). Source–receptor relationships for airborne measurements of CO<sub>2</sub>, CO and O<sub>3</sub> above Siberia: A cluster-based approach. *Atmospheric Chemistry and Physics*, 10, 1671–1687. <https://doi.org/10.5194/acp-10-1671-2010>
- Parrish, D. D., Fahey, D. W., Williams, E. J., Liu, S. C., Trainer, M., Murphy, P. C., et al. (1986). Background ozone and anthropogenic ozone enhancement at Niwot Ridge, Colorado. *Journal of Atmospheric Chemistry*, 4, 63–80. <https://doi.org/10.1007/BF00053773>
- Parrish, D. D., Law, K. S., Staehelin, J., Derwent, R., Cooper, O. R., Tanimoto, H., et al. (2013). Lower tropospheric ozone at northern midlatitudes: Changing seasonal cycle. *Geophysical Research Letters*, 40(8), 1631–1636. <https://doi.org/10.1002/grl.50303>
- Penkett, S. A., & Brice, K. A. (1986). The spring maximum in photo-oxidants in the Northern Hemisphere. *Nature*, 319, 655–657. <https://doi.org/10.1038/319655a0>
- Pochanart, P., Akimoto, H., Kajii, Y., Potemkin, V. M., & Khodzher, T. V. (2003). Regional background ozone and carbon monoxide variations in remote Siberia/East Asia. *Journal of Geophysical Research*, 108(D1), 4028. <https://doi.org/10.1029/2001JD001412>



- Ponomarev, E., Kharuk, V. I., & Ranson, K. J. (2016). Wildfires dynamics in Siberian larch forests. *Forests*, 7, 125. <https://doi.org/10.3390/f7060125>
- Potemkin, V. L., Golobokova, L. P., & Khodzher, T. V. (2019). Climatology and chemistry of surface ozone and aerosol under alpine conditions in East Siberia. *Aerosol and Air Quality Research*, 19, 1214–1225. <https://doi.org/10.4209/aaqr.2018.05.0172>
- Pusede, S. E., Gentner, D. R., Wooldridge, P. J., Browne, E. C., Rollins, A. W., Min, K.-E., et al. (2014). On the temperature dependence of organic reactivity, nitrogen oxides, ozone production, and the impact of emission controls in San Joaquin Valley, California. *Atmospheric Chemistry and Physics*, 14, 3373–3395. <https://doi.org/10.5194/acp-14-3373-2014>
- Romer, P. S., Duffey, K. C., Wooldridge, P. J., Edgerton, E., Baumann, K., Feiner, P. A., et al. (2018). Effects of temperature-dependent NO<sub>x</sub> emissions on continental ozone production. *Atmospheric Chemistry and Physics*, 18, 2601–2614. <https://doi.org/10.5194/acp-18-2601-2018>
- Schindlbacher, A. (2004). Effects of soil moisture and temperature on NO, NO<sub>2</sub>, and N<sub>2</sub>O emissions from European forest soils. *Journal of Geophysical Research*, 109(D17). <https://doi.org/10.1029/2004jd004590>
- Shtabkin, Y. A., Moiseenko, K. B., Skorokhod, A. I., Vasileva, A. V., & Heimann, M. (2016). Sources of and variations in tropospheric CO in Central Siberia: Numerical experiments and observations at the Zotino Tall Tower Observatory. *Izvestiya, Atmospheric and Oceanic Physics*, 52(1), 45–56. <https://doi.org/10.1134/s0001433816010096>
- Singh, H. B., Ludwig, F. L., & Johnson, W. B. (1978). Tropospheric ozone: Concentrations and variabilities in clean remote atmospheres. *Atmospheric Environment*, 12(11), 2185–2196. [https://doi.org/10.1016/0004-6981\(78\)90174-9](https://doi.org/10.1016/0004-6981(78)90174-9)
- Solberg, S., Stordal, F., & Hov, Ø. (1997). Tropospheric ozone at high latitudes in clean and polluted air masses, a climatological study. *Journal of Atmospheric Chemistry*, 28, 111–123. <https://doi.org/10.1023/A:1005766612853>
- Tanimoto, H., Matsumoto, K., & Uematsu, M. (2008). Ozone–CO correlations in Siberian wildfire plumes observed at Rishiri Island. *SOLA*, 4, 65–68. <https://doi.org/10.2151/SOLA.2008-017>
- Thorp, T., Arnold, S. R., Pope, R. J., Spracklen, D. V., Conibear, L., Knote, C., et al. (2020). Late-spring and summertime tropospheric ozone and NO<sub>2</sub> in Western Siberia and the Russian Arctic: Regional model evaluation and sensitivities. *Atmospheric Chemistry and Physics*. <https://doi.org/10.5194/acp-2020-426>
- Timokhina, A. V., Prokushkin, A. S., Panov, A. V., Kolosov, R. A., Sidenko, N. V., Lavric, J. V., & Heimann, M. (2018). Interannual variability of atmospheric CO<sub>2</sub> concentrations over central Siberia from ZOTTO data for 2009–2015. *Russian Meteorology and Hydrology*, 43(5), 288–294. <https://doi.org/10.3103/S1068373918050023>
- Trainer, M., Hsie, E. Y., McKeen, S. A., Tallamraju, R., Parrish, D. D., Fehsenfeld, F. C., & Liu, S. C. (1987). Impact of natural hydrocarbons on hydroxyl and peroxy radicals at a remote site. *Journal of Geophysical Research*, 92(D10), 11879–11894. <https://doi.org/10.1029/JD092iD10p11879>
- Trainer, M., Williams, E., Parrish, D., Buhr, M. P., Allwine, E. J., Westberg, H. H., et al. (1987). Models and observations of the impact of natural hydrocarbons on rural ozone. *Nature*, 329, 705–707. <https://doi.org/10.1038/329705a0>
- Tripathi, O. P., Jennings, S. G., O'Dowd, C., O'Leary, B., Lambkin, K., Moran, E., et al. (2012). An assessment of the surface ozone trend in Ireland relevant to air pollution and environmental protection. *Atmospheric Pollution Research*, 3(3), 341–351. <https://doi.org/10.5094/APR.2012.038>
- Turner, M. C., Jerrett, M., Pope, C. A., Krewski, D., Gapstur, S. M., Diver, W. R., et al. (2016). Long-term ozone exposure and mortality in a large prospective study. *American Journal of Respiratory and Critical Care Medicine*, 193(10), 1134–1142. <https://doi.org/10.1164/rccm.201508-1633OC>
- van der Werf, G. R., Randerson, J. T., Giglio, L., van Leeuwen, T. T., Chen, Y., Rogers, B. M., et al. (2017). Global fire emissions estimates during 1997–2016. *Earth System Science Data*, 9, 697–720. <https://doi.org/10.5194/essd-9-697-2017>
- Vasconcelos, L. A. P., Kahl, J. D. W., Liu, D., Macias, E. S., & White, W. H. (1996). A tracer calibration of back trajectory analysis at the Grand Canyon. *Journal of Geophysical Research*, 101(D14), 329–419. <https://doi.org/10.1029/95JD02609>
- Vasileva, A., Moiseenko, K., Skorokhod, A., Belikov, I., Kopeikin, V., & Lavrova, O. (2017). Emission ratios of trace gases and particles for Siberian forest fires on the basis of mobile ground observations. *Atmospheric Chemistry and Physics*, 17, 12303–12325. <https://doi.org/10.5194/acp-17-12303-2017>
- Vasileva, A. V., Moiseenko, K. B., Mayer, J.-C., Jürgens, N., Panov, A., Heimann, M., & Andreae, M. O. (2011). Assessment of the regional atmospheric impact of wildfire emissions based on CO observations at the ZOTTO tall tower station in central Siberia. *Journal of Geophysical Research*, 116. D07301. <https://doi.org/10.1029/2010JD014571>
- Vasileva, A. V., Moiseenko, K. B., & Pankratova, N. V. (2010). Estimates of carbon monoxide emissions from wildfires in northern Eurasia for airquality assessment and climate modeling. *Izvestiya, Atmospheric and Oceanic Physics*, 46, 281–293. <https://doi.org/10.1134/S0001433810030023>
- Vingarzan, R. (2004). A review of surface ozone background levels and trends. *Atmospheric Environment*, 38, 3431–3442. <https://doi.org/10.1016/j.atmosenv.2004.03.030>
- Wang, B., Shugart, H. H., Shuman, J. K., & Lerdau, M. T. (2016). Forests and ozone: Productivity, carbon storage and feedbacks. *Scientific Reports*, 6, 22133. <https://doi.org/10.1038/srep22133>
- Wild, O., Pochanart, P., & Akimoto, H. (2004). Trans-Eurasian transport of ozone and its precursors. *Journal of Geophysical Research*, 109(D11). <https://doi.org/10.1029/2003JD004501>
- Wolfe, G. M., Thornton, J. A., McKay, M., & Goldstein, A. H. (2011). Forest-atmosphere exchange of ozone: Sensitivity to very reactive biogenic VOC emissions and implications for in-canopy photochemistry. *Atmospheric Chemistry and Physics*, 11, 7875–7891. <https://doi.org/10.5194/acp-11-7875-2011>